

Enhanced Joint Sparsity via Iterative Support Detection

Ya-Ru Fan^a, Yilun Wang^{a,b,c,**}, Ting-Zhu Huang^a

^a *School of Mathematical Sciences, University of Electronic Science and Technology of China, Chengdu, Sichuan, 611731 China*

^b *Center for Information in Biomedicine, University of Electronic Science and Technology of China, Chengdu, Sichuan, 610054 P. R. China.*

^c *Center for Applied Mathematics, Cornell University, Ithaca, NY, 14853, USA*

Abstract

Joint sparsity has attracted considerable attention in recent years in many fields including sparse signal recovery in compressed sensing (CS), statistics, and machine learning. Traditional convex models suffer from the suboptimal performance though enjoying tractable computation. In this paper, we propose a new non-convex joint sparsity model, and develop a corresponding multi-stage adaptive convex relaxation algorithm. This method extends the idea of iterative support detection (ISD) from the single vector estimation to the multi-vector estimation by considering the joint sparsity prior. We provide some preliminary theoretical analysis including convergence analysis and a sufficient recovery condition. Numerical experiments from both compressive sensing and feature learning show the better performance of the proposed method in comparison with several state-of-the-art alternatives. Moreover, we demonstrate that the extension of ISD from the single vector to multi-vector estimation is not trivial. In particular, while ISD does not work well for reconstructing the signal channel sparse Bernoulli signal, it does achieve significantly improved performance when recovering the multi-channel sparse Bernoulli signal thanks to its ability of natural incorporation of the joint sparsity structure.

Keywords: Compressed sensing, iterative support detection, joint sparsity,

*This work is supported by the 973 project (No. 2015CB856000), the Natural Science Foundation of China (11201054, 91330201) and the Fundamental Research Funds for the Central Universities (ZYGX2013Z005).

**Corresponding author

Email address: yilun.wang@rice.edu (Yilun Wang)

1. Introduction and Contributions

1.1. Brief Introduction to Joint Sparsity

In the last decade, sparsity made it possible for us to reconstruct the high dimensional data with just few samples or measurements. The key point of the sparse estimation problem is to address the identification of the support, which denotes the indices of the nonzeros. If the support is known, the estimation of the sparse vectors reduces to a standard overdetermined linear inverse problem [20].

In order to further enhance the estimation, many recent studies tend to consider the structure information of the solutions. For example, “group sparsity” structure [8, 12] widely appears in many applications, where the components of solutions are likely to be either all zero or all nonzero in a group. By making use of the grouping prior, ones aim to decrease the dispersion to facilitate recovering a much better solution. Here, we focus on joint sparsity, which is a special case of the group sparsity. Joint sparsity means that multiple unknown sparse vectors ($x_j \in \mathbb{R}^n$, $j = 1, \dots, l$) share a common unknown nonzero support set. In the following parts, we introduce the background of joint sparsity via two important applications, i.e. compressive sensing and multi-task feature learning.

In compressive sensing, joint sparsity aims to reconstruct unknown signals from m measurement vectors based on a common measurement matrix. This is also called the multiple measurement vectors (MMV) problem [7, 10, 34]. Given the vectors b_1, \dots, b_l , and a measurement matrix $A \in \mathbb{R}^{m \times n}$, we want to recover the x_j from the noisy underdetermined systems $b_j = Ax_j + e_j$ ($j = 1, \dots, l$), where e_j is the noise vector. The vectors x_1, \dots, x_l share the sparsity pattern M , i.e., the nonzero entries of x_1, \dots, x_l almost appear on the same positions. A common recovery model is

$$\min_X |M| \quad s.t. \quad b_j = Ax_j + e_j, \quad j = 1, \dots, l, \quad (1)$$

where $|M|$ is the cardinality of M [15] and $x_j \in \mathbb{R}^n$ denotes the j -th column of X . We can recover all x_1, \dots, x_l with $\text{rank}[x_1, \dots, x_l] = K$ if and only if

$$|M| < \frac{\text{spark}(A) - 1 + K}{2}, \quad (2)$$

where $\text{spark}(A)$ is the smallest set of linearly dependent columns of A [32]. Since (1) is NP-hard, this problem is usually relaxed with a convex alternative which is computationally efficient at the expenses of more required measurements. Like ℓ_1 -norm being the convex relaxation of ℓ_0 -norm [2], the $\ell_{2,1}$ -norm is widely used as the convex replacement of $|M|$ as below:

$$\min_X \quad \|X\|_{2,1} := \sum_{i=1}^n \|x^i\|_2 \quad (3)$$

$$\text{s.t.} \quad b_j = Ax_j + e_j, j = 1, \dots, l,$$

where $x^i \in \mathbb{R}^l$ and $x_j \in \mathbb{R}^n$ denote the i -th row and the j -th column of X , respectively.

In the field of multi-task feature learning, similar sparse models have also been derived [23, 37]: given l learning tasks associated with training data $\{(A^1, b_1), \dots, (A^l, b_l)\}$, where $A^j \in \mathbb{R}^{m_j \times n}$ is the data matrix of the j -th task with each row as a sample and each column as a feature; $b_j \in \mathbb{R}^{m_j}$ is the response of the j -th task with some biases e_j ; n is the number of features; and m_j is the number of samples for the j -th task. We consider to learn a weight matrix $X = [x_1, \dots, x_l] \in \mathbb{R}^{n \times l}$ ($x_j \in \mathbb{R}^n$ consists of the weight vectors for l linear predictive models $b_j = A^j x_j + e_j$) by the following optimization problem:

$$\min_X \quad \|X\|_{2,1} := \sum_{i=1}^n \|x^i\|_2 \quad (4)$$

$$\text{s.t.} \quad b_j = A^j x_j + e_j, j = 1, \dots, l,$$

where $x^i \in \mathbb{R}^l$ and $x_j \in \mathbb{R}^n$ denote the i -th row and the j -th column of X , respectively. Here we assume that these different tasks share the same significant features, which results in a joint sparsity problem.

The unconstrained formulas corresponding to (3) and (4) can be written as the following unified form

$$\min_X \quad L(X) + \rho \|X\|_{2,1}, \quad (5)$$

where $\rho > 0$ is the regularization parameter, and $L(X)$ is a smooth convex loss function such as the least square loss function or the logistic loss function. For example, $L(X) = \sum_{j=1}^l \|Ax_j - \mathbf{b}_j\|_2^2$ for (3), and $L(X) = \sum_{j=1}^l \frac{1}{m_j} \|A^j \mathbf{x}_j - \mathbf{b}_j\|_2^2$ for (4).

While the convexity of $\ell_{2,1}$ regularization provides computational efficiency, it also gives rise to the inherited bias issue [39]. Similar with the ℓ_1 -norm regularized model which only achieves suboptimal recovery performance compared with the original cardinality regularized model from the theoretical viewpoint [4], $\ell_{2,1}$ -norm regularized model also only achieves sub-optimal performance compared with the cardinally based model (1).

Recently, several computational advances have been made in the non-convex sparse regularization since its performance is better than that of the convex sparse regularization. For example, for the single vector recovery, the non-convex ℓ_p -norm ($0 < p < 1$) based sparsity regularization usually obtains better performance than ℓ_1 -norm based sparsity regularization [5]. For the joint sparsity, the $\ell_{q,p}$ -norm is applied in a similar way, where $0 < p < 1$ and $q \geq 1$. The non-convex sparse regularization needs less strict recovery requirements and usually achieves a better performance than the convex alternatives. While there have existed many algorithms for solving the non-convex sparse regularized models, it is still a challenging problem to obtain the global optimal solution efficiently. In addition, the behavior of a local solution is hard to analyze and more seriously structural information of the solution is also hard to be incorporated into these algorithms.

1.2. Our Contributions

In this paper, we propose a non-convex joint sparsity regularized model and a multi-stage convex relaxation algorithm, in order to achieve a better tradeoff between the recovery quality and the computational efficiency. Our method extends the idea of threshold based iterative support detection (*threshold*-ISD) [33] from common sparsity to joint sparsity, from compressive sensing to feature learning. We present some new insights about why ISD achieves better performance than its convex alternatives, its key differences with other weighting based alternatives, and its flexibility in support detection implementation. Moreover, we provide the preliminary theoretical results including the convergence analysis and a sufficient recovery condition.

More important, we discover some advantages of ISD which are not observed in the single vector recovery case. In specific, for the single channel sparse signal estimation, *threshold*-ISD depends on the assumption of the fast decaying property of the nonzero components of the underlying true sparse signal and does not work for non-decaying signals. However, we empirically show that this assumption is no longer necessary for multi-channel sparse signal recovery, because the joint sparsity structure is adopted in the

specific implementation of support detection. This implies that ISD might be naturally fused with the more general structural sparsity.

1.3. Outline

The paper is organized as follows. In Section 2, we propose a non-convex joint sparsity model and develop a corresponding algorithm based on ISD. In Section 3, some preliminary theoretical results are presented. In Section 4, we provide numerical experiments from compressed sensing and multi-task feature learning to demonstrate the effectiveness of the proposed method. Section 5 is devoted to the conclusion and discussion on some possible future research directions.

2. The Proposed Model and Corresponding Algorithm

We only take the model (3) of compressive sensing as the example to show how ISD is extended to the joint sparsity models due to the length limitation of the paper. Similar idea can be expanded to the multi-task feature learning model (4), as well as the unconstrained version (5).

2.1. Truncated Joint Sparsity Model

The proposed model based on the original joint sparsity model (3) is given as follows:

$$\begin{aligned} \min_{X(\omega)} \quad & \|X\|_{w,2,1} := \sum_{i=1}^n w_i \|x^i\|_2 \\ \text{s.t.} \quad & B = AX + E, \end{aligned} \quad (6)$$

where E is the noise matrix and $w = [w_1, w_2, \dots, w_n]$ is a weight parameter vector. Compared with the model (3), we can see the main difference is the introduction of the weight vector w . Notice that our model prefers a specific 0-1 weighting scheme, i.e. w_i is either 0 or 1, though most existing weighted models define weight as positive continuous real values.

Let T be the set of the indices of the nonzero rows of X , and the model (6) can be rewritten as

$$\begin{aligned} \min_{X(T)} \quad & \|X\|_{T,2,1} := \sum_{i \in T} \|x^i\|_2 \quad (TJS) \\ \text{s.t.} \quad & B = AX + E. \end{aligned} \quad (7)$$

We call it as truncated joint sparsity (TJS) model.

Intuitively, if we believe that x^i is truly nonzero, it should be not forced to move closer to 0 and therefore we remove it from the regularization term, i.e. its corresponding w_i is set as 0. Moreover, while many existing works assume that partial support information about underlying true sparse signal is already known [27, 17, 31], the assumption may not hold in practice because w_i is not given beforehand. ISD, as a self-learning scheme, aims to gradually detect partial support information. It is a multi-stage alternative optimization procedure, which repeatedly applies the following two steps when applied to model (7):

- Step 1: we optimize x^i with w (or T) fixed (initially $\vec{1}$): this is a convex problem in terms of X .
- Step 2: we determine the value of w according to the current X via a support detection operation. The value of w will be used in the Step 1 of the next iteration.

Step 2 estimates the true nonzero rows from the rough intermediate estimated results of Step 1, and therefore called “support detection”. Our algorithm starts from initializing $w^{(0)} = \vec{1}$. In the first iteration, we obtain a solution $X^{(1)}$, which amounts to the solution obtained by solving the plain $\ell_{2,1}$ model (3). Then we obtain the weight $w^{(1)}$ using $X^{(1)}$ as the reference. In the following iterations, we obtain the final solution with the updated weights. Therefore ISD in fact decouples the estimation of w and X by an alternative scheme. We name this multi-stage convex relaxation procedure as iterative support detection based joint sparsity algorithm (ISDJS).

2.2. Step 1: Solving Truncated Joint Sparsity Model

The $\ell_{2,1}$ -norm minimization based joint sparsity model (3) leads to a convex optimization problem, and there are many efficient first-order algorithms depending on different application fields [16, 18, 28, 1, 35, 21], which mostly try to make use of the sparsity of the solutions in varied ways. For compressive sensing, one of the most popular algorithms is the alternating direction method (ADM)[36, 8]. In [36], Yong et al. applied the ADM technique to solving the ℓ_1 problem in compressed sensing and developed the corresponding Matlab package termed Your ALgorithms for L_1 (YALL1). Furthermore, Deng et al. extended the YALL1 to the group version for solving the group sparse optimization with $\ell_{2,1}$ -norm regularization in [8]. For feature learning,

Liu et al. proposed an efficient algorithm based on the Nesterovs method and the Euclidean projection in [22].

It is quite straightforward to extend these methods from $\ell_{2,1}$ -norm based models to truncated or weighted $\ell_{2,1}$ -norm regularized models without much extra work. We take the YALL1 group algorithm for solving the plain $\ell_{2,1}$ regularized compressive sensing model as an example, and the resulted variant of the YALL1 group algorithm for the truncated joint sparsity model (6) is summarized in Algorithm 1.

Algorithm 1 Solving step 1 (The Inner Iteration)

1. Initialize $X \in R^{n \times l}$, $\Lambda_1 \in R^{n \times l}$, $\Lambda_2 \in R^{m \times l} > 0$,
 $\beta_1, \beta_2 > 0$ and $\gamma_1, \gamma_2 > 0$;
 2. While stopping criterion is not met, do
 - (a) $X \leftarrow (\beta_1 I + \beta_2 A^T A)^{-1}(\beta_1 Z - \Lambda_1 + \beta_2 A^T B + A^T \Lambda_2)$,
 - (b) $Z \leftarrow \text{Shrink}(X + \frac{1}{\beta_1} \Lambda_1, \frac{1}{\beta_1} w)$,
 - (c) $\Lambda_1 \leftarrow \Lambda_1 - \gamma_1 \beta_1 (Z - X)$,
 - (d) $\Lambda_2 \leftarrow \Lambda_2 - \gamma_2 \beta_2 (AX - B)$,
 where Λ_1, Λ_2 are multipliers, β_1, β_2 are penalty parameters,
 γ_1, γ_2 are step lengths.
-

Notice that the only modification of the extension of the YALL1 group algorithm from the common joint sparsity to the truncated joint sparsity is the step of updating Z , which is implemented by a shrinkage operator:

$$z^i = \text{Shrink}(r^i, \frac{1}{\beta_1} w) = \max\{\|r^i\|_2 - \frac{w_i}{\beta_1}, 0\} \frac{r^i}{\|r^i\|_2}, \quad i = 1, \dots, n, \quad (8)$$

where

$$r^i := x^i + \frac{1}{\beta_1} \lambda_1^i. \quad (9)$$

The above small modification explains why truncated $\ell_{2,1}$ -norm based model could be better than the $\ell_{2,1}$ alternatives. It is well known that $\ell_{2,1}$ -norm based model, as its counterpart of ℓ_1 -norm based model, suffers from its uniform shrinkage on all its components, i.e. it shrinks the true nonzero components as well, and reduces the sharpness of the solution or introduces bias to the final solution. In fact, the true nonzero components should not be shrunk in order to avoid the possibly caused bias. The truncated model can partially reduce this bias, because it corresponds to a selective shrinkage

procedure where the weight value w_i is either 1 or 0. The true large nonzero components are expected to have the 0 weights and therefore will not be shrunk. Surely we need to have some knowledge about the support information of the underlying true solution in order for the appropriate settings of weights. The support detection is implemented in Step 2, which will be introduced in the following subsection.

2.3. Step 2: Weight Determination Based on the Iterative Support Detection

Step 2 is a key part of the proposed algorithm. As we mentioned above, our strategy obtains the partial support information by itself, rather than given beforehand. Concretely, based on the recent intermediate result, we infer the indexes of nonzero rows of the underlying unknown true solution \bar{X} . Once we believe that certain rows are nonzero in the true solution \bar{X} , we set the corresponding weights to be zeros, and the rest weights are all 1.

Since the intermediate result is not very accurate, a robust way to detect the correct information about the true nonzero rows is required. Some extra prior knowledge of the underlying \bar{X} is needed in order for reliable support detection. Recall that in the single channel sparse signal recovery case, the nonzero components of the sparse or compressible signal are assumed to have a fast decaying distribution for the effectiveness of the threshold based support detection scheme (named *threshold-ISD*). As for the multi-vector estimation problem, *threshold-ISD*, can also be applied in a similar way. At the s -th stage, we have an intermediate solution $X^{(s)}$. We aim to obtain some correct support information about the true \bar{X} based on $X^{(s)}$, i.e. identify some truly nonzero rows. The set of indices of detected nonzero rows based on *threshold-ISD* is similarly defined below:

$$I^{(s+1)} := \{i : |t_i^{(s)}| > \epsilon^{(s)}\}, s = 0, 1, 2, \dots, \quad (10)$$

where $t_i = \|x^i\|_2$. The support set $I^{(s)}$ is not necessarily increasing and nested, which means that all s may be not in $I^{(s)} \subset I^{(s+1)}$. Because $I^{(s)}$ is not required to be monotonic, support detection can remove previous wrong detections, which makes $I^{(s)}$ less sensitive to $\epsilon^{(s)}$.

As for the choice of $\epsilon^{(s)}$, the “first significant jump” heuristic is proposed in the original implementation of ISD [33]. Specifically, ones first sorts sequence $|t_{[i]}^{(s)}|$ in ascending order ($|t_{[i]}^{(s)}|$ denotes the i -th largest component of t by magnitude). The “first significant jump” scheme looks for the smallest i such that

$$|t_{[i+1]}^{(s)}| - |t_{[i]}^{(s)}| > \tau^{(s)}, \quad (11)$$

where $\tau^{(s)}$ is a data-dependent prescribed value to detect the big jump of this sequence. There are several simple and heuristic methods to define $\tau^{(s)}$. For example, one can set

$$\tau^{(s)} = m^{-1} \|t^{(s)}\|_{\infty}, \quad (12)$$

where m is the number of measurements. Then we take $\epsilon^{(s)} = |t_{[i]}^{(s)}|$. Intuitively, the ‘‘first significant jump’’ scheme works well because the true nonzero entries of $t^{(s)}$ are large in magnitude and small in number, while the false ones are large in number and small in magnitude. Therefore, the magnitudes of the true nonzero entries are spread out, while those of the false ones are clustered.

Recall that for sparse Bernoulli signals, where the nonzero components have exactly the same magnitude and do not have the fast decaying property, *threshold*-ISD fails to achieve a better performance than its convex alternative in the single channel recovery case as presented in [33]. However, for the joint sparsity cases, *threshold*-ISD in fact naturally incorporates this extra joint sparsity structure in the implementation of support detection and succeeds achieving a better recovery quality, as presented below in Section 4. The overall procedure of ISDJS is summarized as Algorithm 2.

We need to point out the difference of the 0-1 weighting scheme with a popular weighting method proposed in [2] where the weight is determined as follows:

$$w_i^{(s)} = \frac{1}{|x_i^{(s)}| + \xi},$$

where the choice of $\xi > 0$ is a key for the performance of its corresponding algorithm. If the ξ is too small, then too much noisy information is taken into consideration. If the ξ is too big, much of the information about the true nonzero elements is filtered out. An appropriate way might be to gradually decrease ξ from a large number to a small one as s increases. However, the determination of ξ is hard. While we know ξ should be data-adaptive, a feasible practical scheme to determine ξ is not easy to design. On the contrary, the Step 2 is much easier to obtain a data-adaptive scheme.

In addition, an advantage of the proposed strategy is that the implementation of support detection is very flexible. Besides the above heuristic (12), one can try many other alternative ideas. For example, one dimensional edge detection methods such as those proposed in [38, 3] can also be adopted to detect the ‘‘first significant jump’’, i.e. determine an appropriate $\tau^{(\ell)}$ value for (11). In the following numerical experiments, while the heuristic rule

(12) will be mostly adopted, the real problem in Section 4.3 employs one dimensional edge detection method proposed in [38] as an illustration.

Algorithm 2 The ISDJS algorithm (The Outside Iteration)

Input: A and B ,

1. Set the iteration number $s \leftarrow 1$ and

 initialize $w^{(0)} = \vec{1}$;

2. While stopping condition is not met, do

(a) $X^{(s)} \leftarrow$ solve problem (7) via Algorithm 1 for $w = w^{(s-1)}$;

(b) $w^{(s)} \leftarrow T^{(s)} := (I^{(s)})^C = \{1, 2, \dots, n\} \setminus I^{(s)}$;

 where $I^{(s)} \leftarrow$ compute approach (10) for $X = X^{(s)}$;

(c) $s \leftarrow s + 1$.

Although ISDJS is a multi-stage procedure, its costing time is not necessarily several times of the original $\ell_{2,1}$ model, if the warm-starting scheme is adopted, i.e. the output of the current stage (outside iteration) is used to be the initial point when solving the truncated model of the next stage. In addition, in the intermediate stages, a looser stopping tolerance can be used since a not very accurate intermediate solution is enough for the purpose of support detection. Finally, the stage number is not necessarily large empirically, like around 4 as the following numerical experiments presented in section 4.

3. Preliminary Theoretical Analysis

In this section, we present some preliminary theoretical analysis for the proposed truncated joint sparsity model and the corresponding ISDJS algorithm. We will focus on the convergence analysis and a sufficient recovery condition.

3.1. Convergence Analysis

We assume that $A \in \mathbb{R}^{m \times n}$ and $A^j \in \mathbb{R}^{m_j \times n}$ follow the continuous probability distribution. This convergence analysis applies to both the compressive case and the multi-task feature learning case. In practice, ISDJS only runs a few steps and s is smaller than 5 in general, and these steps can be considered to determine a proper threshold value ϵ for support detection (10). For simplicity of proof, when considering the convergence analysis where s goes to infinity, we assume that the threshold value $\epsilon^{(s)}$ used in support detection

(10) is fixed as $\bar{\epsilon}$ when $s > \bar{s}$ ($\bar{s} = 5$, for example). This assumption is slightly biased from the truth, because the threshold value could keep changing as the iteration of ISDJS proceeds. However, it is also reasonable and acceptable to certain degree because in practice, ISDJS only runs a very limited number of steps, i.e. ISDJS will stop when s is not very big. Moreover, even as s goes to infinity, the threshold value will not change much empirically.

The main idea of the following proof refers to [13]. However, unlike [13] where a truncated $\ell_{1,1}$ model is considered, we consider a truncated $\ell_{2,1}$ model. A locally linear approximation is presented as a preparation for the following convergence proof.

First, for any $\epsilon > 0$, we consider the following unstrained weighted $\ell_{2,1}$ regularized model corresponding to (5):

$$\min_X L(X) + \rho \sum_{i=1}^n w_i \|\mathbf{x}^i\|_2 \quad (13)$$

where $L(X)$ is a quadratic cost function of X and $\rho(> 0)$ is a parameter. In terms of ISDJS algorithm we denote $w_i = T(\|\mathbf{x}^i\|_2 < \epsilon)$ and $T(\cdot)$ denotes the $\{0, 1\}$ -valued indicator function, which is consistent with $T = I^C$ in Algorithm 2.

The solution of problem (13) is equivalent to the solution of the following problem:

$$\min_X L(X) + \rho \sum_{i=1}^n \min(\|\mathbf{x}^i\|_2, \epsilon) \quad (14)$$

We assume that $\epsilon^{(s)}$ is kept unchanged after several steps of ISDJS. That is to say when s is big enough, $\epsilon^{(s)} \doteq \bar{\epsilon}$ in Algorithm 2.

Second, we define two auxiliary functions:

$$\mathbf{h} : R^{n \times l} \mapsto R_+^n, \mathbf{h}(X) = [\|\mathbf{x}^1\|_2, \|\mathbf{x}^2\|_2, \dots, \|\mathbf{x}^n\|_2]^T, \quad (15)$$

$$g_\epsilon : R_+^n \mapsto R_+, g_\epsilon(\mathbf{u}) = \sum_{i=1}^n \min(u_i, \epsilon). \quad (16)$$

Note that $g_\epsilon(\cdot)$ is a concave function [13]. (When s is large enough, $g_{\epsilon^{(s)}} = g_{\bar{\epsilon}}$.) We know that a vector $\mathbf{z} \in R^n$ is a sub-gradient of g at $\mathbf{v} \in R_+^n$, if for all vector $\mathbf{u} \in R_+^n$, the following inequality holds:

$$g_\epsilon(\mathbf{u}) \leq g_\epsilon(\mathbf{v}) + \langle \mathbf{z}, \mathbf{u} - \mathbf{v} \rangle, \quad (17)$$

where $\langle \cdot, \cdot \rangle$ denotes the inner product. Based on the functions defined above, problem (14) is equivalent to the following problem

$$\min_X L(X) + \rho g_\epsilon(\mathbf{h}(X)). \quad (18)$$

Then we can obtain an upper bound of $g_\epsilon(\mathbf{h}(X))$ using a locally linear approximation at $\mathbf{h}(X^{(s)})$ based on the inequality (17):

$$g_\epsilon(\mathbf{h}(X)) \leq g_{\epsilon^{(s)}}(\mathbf{h}(X^{(s)})) + \langle \mathbf{z}^{(s)}, \mathbf{h}(X) - \mathbf{h}(X^{(s)}) \rangle, \quad (19)$$

where $\mathbf{z}^{(s)} = [T(\|\mathbf{x}^{(s)1}\|_2 < \epsilon), \dots, T(\|\mathbf{x}^{(s)n}\|_2 < \epsilon)]^T$ is a sub-gradient of $g_\epsilon(\mathbf{u})$ at $\mathbf{u} = \mathbf{h}(X^{(s)})$. Furthermore, for $\forall \mathbf{h}(X)$ we obtain an upper bound of the optimization problem (14):

$$L(X) + \rho g_\epsilon(\mathbf{h}(X)) \leq L(X) + \rho g_{\epsilon^{(s)}}(\mathbf{h}(X^{(s)})) + \rho \langle \mathbf{z}^{(s)}, \mathbf{h}(X) - \mathbf{h}(X^{(s)}) \rangle. \quad (20)$$

Since ρ and $h(X^{(s)})$ are constant with respect to X , we have

$$\begin{aligned} X^{(s+1)} &= \arg \min_X L(X) + \rho g_{\epsilon^{(s)}}(\mathbf{h}(X^{(s)})) + \rho \langle \mathbf{z}^{(s)}, \mathbf{h}(X) - \mathbf{h}(X^{(s)}) \rangle \\ &= \arg \min_X L(X) + \rho (\mathbf{z}^{(s)})^T \mathbf{h}(X), \end{aligned} \quad (21)$$

which corresponds to the step 2 (a) of the Algorithm 2. Therefore, we intuitively consider that the Algorithm 2 minimizes an upper bound in each step.

Theorem 1 Let $\bar{f}(X) = L(X) + \rho \sum_{i=1}^n \bar{w}_i \|\mathbf{x}^i\|_2$, where $\bar{w}_i = T(\|\mathbf{x}^i\|_2 < \bar{\epsilon})$. The sequence $\{\bar{f}(X^{(s)})\}$ is decreasing and convergent.

Proof When s is big enough, $\epsilon^{(s)} = \bar{\epsilon}$, and $g_{\epsilon^{(s)}} = g_{\bar{\epsilon}}$. We firstly verify the objective function value in (14) decreases monotonically based on locally linear approximation, when s is big enough, as follows:

$$\begin{aligned} L(X^{(s+1)}) + \rho g_{\bar{\epsilon}}(\mathbf{h}(X^{(s+1)})) &\leq L(X^{(s+1)}) + \rho g_{\bar{\epsilon}}(\mathbf{h}(X^{(s)})) + \rho \langle \mathbf{z}^{(s)}, \mathbf{h}(X^{(s+1)}) - \mathbf{h}(X^{(s)}) \rangle \\ &\leq L(X^{(s)}) + \rho g_{\bar{\epsilon}}(\mathbf{h}(X^{(s)})) + \rho \langle \mathbf{z}^{(s)}, \mathbf{h}(X^{(s)}) - \mathbf{h}(X^{(s)}) \rangle \\ &= L(X^{(s)}) + \rho g_{\bar{\epsilon}}(\mathbf{h}(X^{(s)})), \end{aligned}$$

where the first inequality is based on Equation (20) and the second inequality follows (21), i.e., $X^{(s+1)}$ is a minimizer of the right hand side of Equation (20). Then we have

$$\bar{f}(X^{(s+1)}) \leq \bar{f}(X^{(s)}).$$

Obviously, we observe that

$$\bar{f}(X) = L(X) + \rho \sum_{i=1}^n \bar{w}_i \|\mathbf{x}^i\|_2 \geq 0.$$

Thus $\{\bar{f}(X^{(s)})\}$ is bounded below. Therefore $\{\bar{f}(X^{(s)})\}$ is convergent.

■

3.2. A Sufficient Recovery Condition of TJS Model

Here we consider the noiseless compressive sensing model (3). We first revisit the truncated null space property (t-NSP) proposed in [33], which is a generalization of the null space property (NSP).

Definition 1. *Matrix A satisfies the t -NSP of order L for $\gamma > 0$ and $0 < t \leq n$ if*

$$\|\eta_S\|_1 \leq \gamma \|\eta_{(T \cap S^c)}\|_1 \quad (22)$$

holds for all sets $T \subset \{1, \dots, n\}$ with $|T| = t$, all subsets $S \subset T$ with $|S| \leq L$, and all $\eta \in \mathcal{N}(A)$ — the null space of A .

For simplicity, we use t -NSP(t, L, γ) to denote the t -NSP of order L for γ and t , and use $\bar{\gamma}$ to replace γ and write t -NSP($t, L, \bar{\gamma}$) if $\bar{\gamma}$ is the infimum of all the feasible γ satisfying (22).

For the single channel sparse signal recovery problem

$$\begin{aligned} \min_x \quad & \|x_T\|_1 \\ \text{s.t.} \quad & b = Ax \end{aligned} \quad (23)$$

Theorem 3.2 in [33] has shown that if $A \in \mathbb{R}^{m \times n}$ ($m < n$) satisfies the t -NSP, then the true signal \bar{x} is the unique solution of model (23) if

$$\|\bar{x}_T\|_0 < k(d), \quad (24)$$

where $k(d) := c \frac{m-d}{1+\log(\frac{n-d}{m-d})}$, $d = n - t = n - |T|$, and $c > 0$ is absolute constant independent of the dimensions m , n and d . Let $d_c = |I \cap \text{supp}(\bar{t})|$ stand for the number of correct detections, and inequality (24) is equivalent to

$$\|\bar{x}\|_0 < k(d) + d_c, \quad (25)$$

due to $\|\bar{x}\|_0 = \|\bar{x}_T\|_0 + d_c$. In light of (25), to compare the common ℓ_1 model with truncated ℓ_1 model (23), we shall compare $k(0)$ with $k(d) + d_c$. In [33], the authors have shown that if there are enough correct detections (i.e., d_c/d is sufficiently large), then we get $k(0) < k(d) + d_c$. That is to say, the truncated ℓ_1 model might be able to recovery more nonzeros than the common ℓ_1 model. We extend the above conclusion about the advantage of the truncated ℓ_1 model over the common ℓ_1 model from the single vector case to the multi-vector recovery case, i.e. the joint sparsity case. We will see that this kind of extension is feasible thanks to the theorem proved in [19], which is revisited below.

Theorem 1.3 in [19] has proved the following two statements are equivalent.

(a) for all vectors $(\mathbf{u}^1, \dots, \mathbf{u}^r) \in (\mathcal{N}(A))^r \setminus \{(0, 0, \dots, 0)\}$

$$\sum_{j \in S} (\sqrt{u_{1,j}^2 + \dots + u_{r,j}^2}) < \sum_{j \in S^c} (\sqrt{u_{1,j}^2 + \dots + u_{r,j}^2}), \quad (26)$$

(b) for all vector $\mathbf{v} \in \mathcal{N}(A)$ with $v \neq 0$

$$\sum_{j \in S} |v_j| < \sum_{j \in S^c} |v_j|, \mathbf{v} = (v_1, \dots, v_n)^T \in R^n \quad (27)$$

hold for all index sets $S \subset \{1, 2, \dots, n\}$ with $|S| \leq L$, where $\mathcal{N}(A)$ stands for the null space of A and S^c is the complement set of S . Namely, the null space property of multiple systems of linear equations is equivalent to the null space property for the comm ℓ_1 minimization subject to a single linear system.

During their proof of this equivalence, they only make use of the fact $S \cap S^c = \emptyset$. So we naturally have the following equivalence [19]:

(c) for all vectors $(\mathbf{u}^1, \dots, \mathbf{u}^r) \in (\mathcal{N}(A))^r \setminus \{(0, 0, \dots, 0)\}$

$$\sum_{j \in S} (\sqrt{u_{1,j}^2 + \dots + u_{r,j}^2}) < \sum_{j \in T \cap S^c} (\sqrt{u_{1,j}^2 + \dots + u_{r,j}^2}), \quad (28)$$

(d) for all vector $\mathbf{v} \in \mathcal{N}(A)$ with $v \neq 0$

$$\sum_{j \in S} |v_j| < \sum_{j \in T \cap S^c} |v_j|, \mathbf{v} = (v_1, \dots, v_n)^T \in R^n \quad (29)$$

hold for all index sets $S \subset \{1, 2, \dots, n\}$ with $|S| \leq L$. Thus, we similarly have the equivalence of the t-NSP of multiple systems of linear equations

with the t-NSP for the common ℓ_1 minimization subject to a single linear system .

Therefore, the better recovery performance of the truncated ℓ_1 model over the common ℓ_1 model can be extended to our specific joint sparsity case, i.e. the multiple-vector compressive sensing problem. Namely, if there are enough correct detections, the truncated joint sparsity model (6) can recover more nonzero rows than the common $\ell_{2,1}$ model, based on the above simple and a little bit intuitive analysis. However, for multi-task learning problem, where different A_j exist, the theoretical judgement of the truncated ℓ_1 model over the common ℓ_1 model needs further investigation.

4. Numerical Experiments

In this section, we present several numerical experiments to demonstrate the better performance of the proposed ISDJS in comparison with several state-of-the-art algorithms. For compressive sensing, we compare with the YALL1 group algorithm [8], SOMP algorithm [32, 9] and p-threshold algorithm [14]. For multi-task feature learning, ISDJS is compared with the baseline algorithm for the common $\ell_{2,1}$ regularized model, whose baseline algorithm proposed in [22] is implemented in the software ‘‘MALSAR’’ [40]. We mainly focus on the recovery rate and accuracy in this paper. Considering that the channel number has a great influence on recovery rate of joint sparsity, we provide several different channel number settings. We also test different noise levels. The synthetic experiments and two realistic experiments from collaborative spectrum sensing [24] and multi-task feature learning, verify the effectiveness of ISDJS.

4.1. Parameter Settings of Synthetic Examples

Two synthetic examples are presented in the context of compressive sensing. The true jointly sparse solution $\bar{X} \in R^{n \times l}$ is generated by randomly selecting k rows as nonzero rows whose entries follow the i.i.d Gaussian and Bernoulli distribution in test 1 and in test 2, respectively. The rest rows of \bar{X} are set as zero. Randomized partial Walsh-Hadamard transform matrix is utilized as the measurement matrix $A \in R^{m \times n}$ in compressive sensing, because it is suitable for large-scale computation and have the property $AA^T = I$. For SOMP and p-thresholding algorithms, we use their default parameter settings in [32, 14]. We set the parameters of the YALL1 group algorithm and ISDJS referring to [8] as follows: $\beta_1 = 0.3 / \frac{1}{ml} \sum_{i=1}^m \sum_{j=1}^l |b_{ij}|$,

$\beta_2 = 3/\frac{1}{ml} \sum_{i=1}^m \sum_{j=1}^l |b_{ij}|$ (b_{ij} is the entries of matrix $B \in R^{m \times l}$) and $\gamma_1 = \gamma_2 = 1.618$. All involved algorithms are terminated when

$$\frac{\|t^{(k+1)} - t^{(k)}\|}{\|t^{(k+1)}\|} \leq \varepsilon. \quad (30)$$

For SOMP, p-threshold and YALL1 group algorithms, ε is set as 10^{-6} . As for ISDJS, for the first few outside iterations, we only want to get an rough estimate of the support information of X , thus we just set a relatively loose tolerance such as $\varepsilon = 10^{-2}$. But for the last step, ε is also set as 10^{-6} for fair comparison. In all experiments, ISDJS runs no more than 5 outer iterations.

The empirical recovery performance of the tested algorithms in general becomes better as the number of channels gradually increases, though to varying degrees [11]. Therefore, different channel number settings are tried in our experiments, for example, $L = 1, 2, 4, 8, 16$, respectively. We also try different sparsity levels varying from $k = 80$ to 160, while fixing $n = 1024$, $m = 256$ in all tests excluding Figure 1, 2, 6, 7. The experimental results corresponding to compressive sensing are usually an average of 100 runs due to the involved randomness in the generation of A and \bar{X} .

4.1.1. Test 1: Compressive Recovery of Joint Sparse Gaussian Signals

We perform a synthetic compressive sensing example to demonstrate some key aspects of ISDJS including the effectiveness of threshold based support detection, the effect of the channel number. We also illustrate how ISDJS produces gradually improved intermediate solutions starting from the low quality initial point which is the solution of the convex alternative. We generate a sparse signal $\bar{X} \in R^{600 \times L}$ with $k = 30$ nonzero rows. The results of ISDJS in the first iteration and the fourth iteration for different channel numbers settings are depicted in the Figure 1, where we set \bar{t} (a vector of 2-norm of each row of \bar{X}) on behalf of the true signal \bar{X} and t (a vector of 2-norm of each row of X from ISDJS) on behalf of the recovered signal. We use the quadruplet “(Total, Detected, Correct, False)” and “Err” defined below to measure the accuracy of support detection.

- (Total, Detected, Correct, False):
 - Total: the number of total nonzero rows of the true signal \bar{X} ;
 - Detected: the number of detected nonzero rows, equal to $|I| = (Correct) + (False)$;
 - Correct: the number of correctly detected nonzero rows, i.e., $|I \cap \{i : \bar{t}^i \neq 0\}|$

0}];

- False: the number of falsely detected nonzero rows , i.e., $|I \cap \{i : \bar{t}^i = 0\}|$.
- Err: the relative error $\|X - \bar{X}\|_2 / \|\bar{X}\|_2$.

From Figure 1 (a), we can see that the output of the first iteration of ISDJS, which is the solution of the common convex $\ell_{2,1}$ -norm regularized model (3), is not good. Nevertheless the output of the fourth iteration of ISDJS could well match the true signal with a very small relative error. We also see that ISDJS is insensitive to a small number of false detections and has an attractive self-correction capacity. In particular, while it is difficult for the common $\ell_{2,1}$ model (3) to recover a signal with 30 nonzero entries from 60 measurements, ISDJS can finally return a satisfying result, as presented in Figure 1 (e). Notice that when the measurements m decrease, ISDJS still returns a better result with channel numbers L increasing.

In order to better understand ISDJS, we show each outer iteration of it in Figure 2, by taking an example of $L = 4$. From the Figure 2 (a), we can see that ISDJS in the first iteration (i.e. YALL1 group algorithm), finds very few positions of correct nonzero rows and has a large relative error. However, a half positions of correct nonzero rows could be detected in the next iteration as exhibited in 2 (b), and a significantly improved recovery is obtained, showed in Figure 2 (c). In the third iteration, our algorithm has already correctly detected the most nonzero positions, and therefore a good enough solution is returned showed in Figure 2 (d).

Figure 3 shows the recovery performance of ISDJS with different channel number settings in four different noise levels to present the robustness of ISDJS to noise. As expected, ISDJS performs better in case of multi-channel sparse signal recovery than the single channel case even in the high level noise.

In Figure 4 and Figure 5, we compare the recovery rates and relative errors of ISDJS with YALL1 group algorithm, SOMP algorithm and p-threshold algorithm, for noiseless case and noisy case (0.5% Gaussian noise), respectively, when the channel number varies. We can see that ISDJS outperforms these alternatives in all the involved different channel numbers settings. Notice that while the common $\ell_{2,1}$ model behaviors worse than the SOMP algorithm in the cases of 4 channels and 8 channels, ISDJS which applies ISD to the common $\ell_{2,1}$ model, behaviors better than SOMP.

4.1.2. Test 2: Compressive Recovery of Joint Sparse Bernoulli Signals

We show a surprising performance of ISD in case of joint sparsity. Recall that for the single channel signal recovery in [33], the *threshold*-ISD works well for signals with a fast decaying property of nonzero entries such as sparse Gaussian signals and certain power-law decaying signals. However, it does not work for signals that decay slowly or have no decay at all such as sparse Bernoulli signals, since the threshold based support detection fail to accurately distinguish true nonzero components according to the intermediate recovery results. As Figure 6 (a) (corresponding to the second row of the table) presented, the support detection is poor and fails to correctly detect the true nonzero entries in the case of the single channel signal recovery. Nevertheless, Figure 6 (b) (corresponding to the third row of the table) shows the threshold based support detection can relatively accurately find some true nonzero rows, even just for $L = 2$. Similarly, in Figures 6 (c) (corresponding to the fourth row of the table), (d) (corresponding to the fifth row of the table) and (e) (corresponding to the sixth row of the table), threshold based support detection works well. Then, the ISDJS achieves quite good recovery performance finally, which suggests that ISD is able to achieve relatively accurate support detection even for Bernoulli signals by incorporating the joint sparsity structure.

In Figure 7, we exhibit the performance of ISDJS for sparse Bernoulli signals of each outer iteration by taking $L=4$ as an example. It is possible to add more iterations but four iterations are enough for ISDJS to return an accurate solution in this case.

In Figure 8, we show the recovery rates of ISDJS with different channel number settings under four noise levels. The ISDJS consistently performs much better in multichannel cases rather than the single channel case. In addition, the ISDJS keeps robust in different levels of noise.

Figure 9 presents the recovery rate of the ISDJS in comparison with other three algorithms for noiseless sparse Bernoulli signals. Figure 9 (a) show that all test algorithms perform poor on single channel Bernoulli signals, since the joint structure prior of signals do not exist here. Surprisingly, the recoverability of ISDJS is dramatically improved as the channel numbers increases in Figure 9 (b), (c), (d) and (e). Similarly, Figure 10 exhibits the relative error of ISDJS compared with the above three algorithms with 0.5% noise level in different channel number settings.

All above numerical experiments attest that ISDJS can make significant

improvement for multichannel sparse signal recovery even without the fast decaying property, by incorporating joint sparsity property into the implementation of threshold based support detection.

4.2. An Example from Collaborative Spectrum Sensing

Here we consider a compressive spectrum sensing scheme for cognitive radio networks [24, 6, 25]. Spectrum sensing aim to detect spectrum holes (i.e., channels not used by any primary users). The cognitive radio (CR) nodes must constantly sense the spectrum in order to detect the presence of the primary radio (PR) nodes and use the spectrum holes without causing harmful interference to the PRs. In practice, improving the ability of detecting complete spectrum usage in collaborative spectrum sensing is an important topic but also a major challenge in CR networks.

We view a l -node cognitive radio network within a 500×500 meter square area centered at the fusion center. The l CR nodes are uniformly randomly located. These cognitive radio nodes collaboratively sense the existence of primary users within a 1000×1000 meter square area on n channels, which are centered also at the fusion center. A channel is either occupied by a PR or unoccupied, corresponding to the states 1 and 0, respectively. Let an $n \times n$ diagonal matrix H represent the states of all the channel sources using 0 and 1 as diagonal entries, indicating the unoccupied or occupied states, respectively. Channel gains are characterized by an $l \times n$ channel gain matrix G . Then, the collaborative spectrum sensing model can be formulated as follows [24]:

$$X_{n \times l} = H_{n \times n}(G_{l \times n})^T. \quad (31)$$

For X , the j -th column of X corresponds to the channel occupancy status received by the j -th CR, and the i -th row of X corresponds to the occupancy status of the i -th channel. A row has a positive value if and only if the i -th channel is used. Since there are only a small number of used channels, X is sparse in terms of the number of nonzero rows. In this example, we set $n = 25$ and $l = 1, 2, 4, 8, 16$. We use the ISDJS algorithm to solve above collaborative spectrum sensing model. Figure 11 presents the results of ISDJS compared with YALL1 group algorithm, SOMP algorithm and p-threshold algorithm in different settings of l . With the sparsity level (nonzero rows) of X increasing, we can see that the advantage of ISDJS is notable.

4.3. An Example for Multi-task Feature Learning

We provide an example to demonstrate the performance of ISDJS for multi-task feature learning. We use a real-world data set, i.e. Letter [22, 26] in this experiment. The Letter data set was collected by the MIT Spoken Language Systems Group. It contains 8 default tasks and 45,679 samples, where the letters are represented by 8×16 binary pixel images. This is a typical multi-task feature learning problem.

For our experiment, we compare the baseline algorithm for solving the common $\ell_{2,1}$ regularized model proposed in [22] with ISDJS. When we set ρ around 4.64×10^{-2} , ISDJS achieves a small relative error, as depicted in Figure 12 (a). Furthermore, we randomly extract the training samples from each task with different training ratios (30%, 35%, 40%, 45% and 50%) and use the rest of samples to form the test set. In the Figure 12 (b), we can see that ISDJS performs much better even with a small training ratio. This real-world experimental results of the multi-task feature learning problem further support the effectiveness of ISDJS.

5. Conclusion

In this paper, we have proposed a truncated joint sparsity model and developed an efficient algorithm named ISDJS to enhance the sparse estimation performance. They are applied in the fields of compressive sensing and feature learning. The proposed method is an extension of self-learning based iterative support detection (ISD) from common sparsity to joint sparsity. The joint sparsity structure is naturally incorporated into the implementation of threshold based support detection and in this way the fast decaying property is no longer required. Then, we have elaborated some preliminary results of the convergence analysis and a sufficient recovery condition for the proposed method. Both synthetic and practical experiments demonstrate the better performance of ISDJS compared with several state-of-the-art alternatives. Future works include designing specific implementations of support detection for different specific problems.

Acknowledgment

The authors would like to thank Dr. Wenxing Zhang for valuable discussion about the theoretical part of the algorithm.

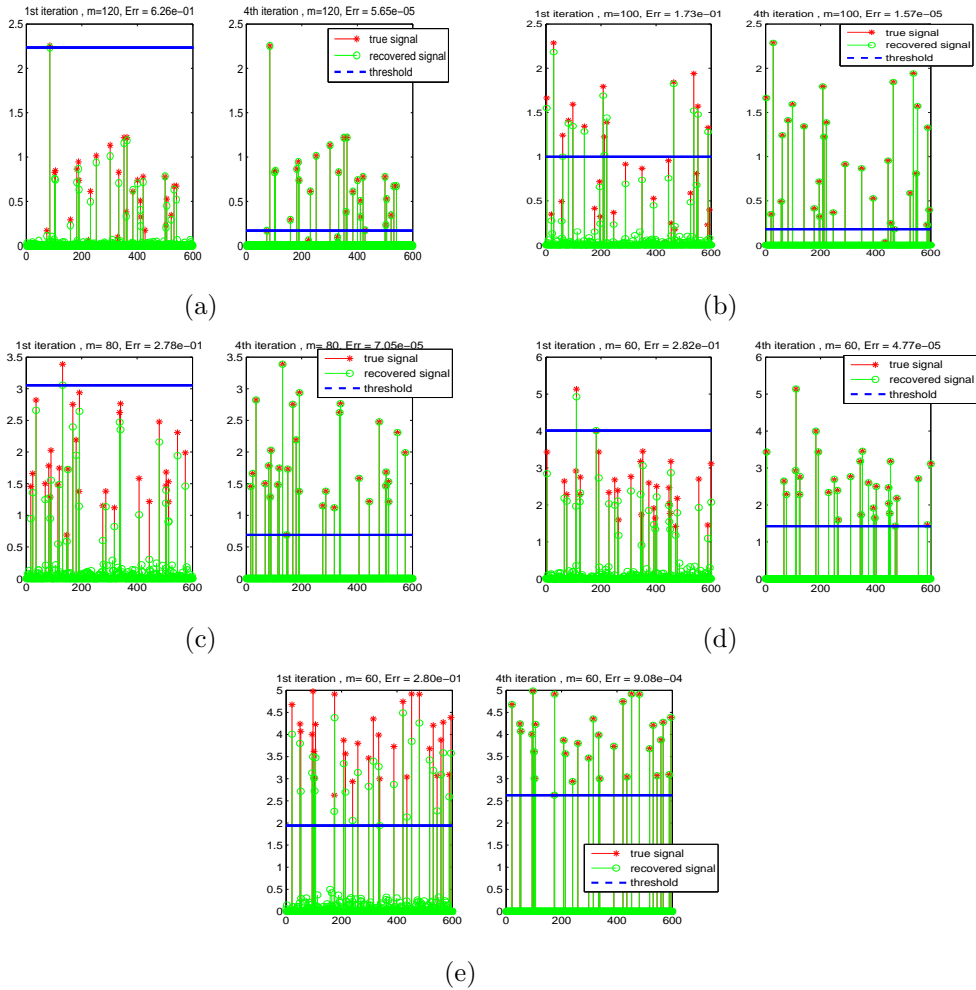
References

- [1] E. D. Berg and M. P. Friedlander, 2009. Joint-sparse recovery from multiple measurements. arXiv preprint, arXiv: 0904. 2051.
- [2] E. J. Candes, M. B. Wakin, and S. P. Boyd, 2008. Enhancing sparsity by reweighted ℓ_1 minimization. *Journal of Fourier Analysis and Applications*, vol. 14, 877-905.
- [3] J. Canny, 1986. A computational approach to edge detection, *IEEE Transactions on Pattern Analysis and Machine Intelligence*, vol. 6, 679-698.
- [4] R. Chartrand and W. Yin, 2008. Iteratively reweighted algorithms for compressive sensing. *International Conference on Acoustics, Speech, and Signal Processing (ICASSP)*, 3869-3872.
- [5] R. Chartrand, 2010. Exact reconstruction of sparse signals via nonconvex minimization. *IEEE Signal Processing Letters*, vol. 14, 707-710.
- [6] Y. Chi, 2014. Joint sparse recovery for spectral compressed sensing. *IEEE International Conference on Acoustic, Speech and Signal Processing (ICASSP)*, 4799-2893.
- [7] S. F. Cotter, B. D. Rao, K. Engan, and K. K. Delgado, 2005. Sparse solutions to linear inverse problems with multiple measurement vectors. *IEEE Transactions on Signal Processing*, vol. 53, no. 7, 2477-2488.
- [8] W. Deng, W. Yin, and Y. Zhang, 2013. Group sparse optimization by alternating direction method. *SPIE Optical Engineering + Applications*. International Society for Optics and Photonics, 88580R-88580R-15.
- [9] M. F. Duarte, S. Sarvotham, D. Baron, M. B. Wakin and R. G. Baraniuk, 2005. Distributed compressed sensing of jointly sparse signals. *Proceedings of the 2005 Asilomar Conference on Signals, Systems, and Computers*.
- [10] M. F. Duarte, S. Sarvotham, M. B. Wakin, D. Baron, and R. G. Baraniuk, 2005. Joint sparsity models for distributed compressed sensing. *Proceedings of the Workshop on Signal Processing with Adaptive Sparse Structured Representations*.

- [11] Y. C. Eldar and H. Rauhut, 2010. Average case analysis of multichannel sparse recovery using convex relaxation. *IEEE Transactions on Information Theory*, vol. 56, 505-519.
- [12] A. R. Gonçalves and P. Das and S. Chatterjee and V. Sivakumar and F. Zuben and A. Banerjee, 2014. Multi-task sparse structure learning. 23rd ACM International Conference on Information and Knowledge Management - CIKM. <http://arxiv.org/abs/1409.0272>
- [13] P. Gong, J. Ye, C. Zhang, 2013. Multi-stage multi-task feature learning. *Journal of Machine Learning Research* 14, 2979-3010.
- [14] R. Gribonval, B. Mailhe, H. Rauhut, K. Schnass and P. Vandergheynst, 2007. Average case analysis of multichannel thresholding. *IEEE International Conference on Acoustic, Speech and Signal Processing (ICASSP)*, 853-856.
- [15] R. Heckel and H. Bolcskei, 2012. Joint sparsity with different measurements matrices. 2012 50th Annual Allerton Conference on Communication, Control, and Computing (Allerton), 698-702.
- [16] M. M. Hyder and K. Mahata, 2009. A robust algorithm for joint-sparse recovery. *IEEE Signal Processing Letters*, vol. 16, no. 12, 1091-1094.
- [17] T. Ince, A. Nacaroglu, and N. Watsuji, 2013. Nonconvex compressed sensing with partially known signal support. *Signal Processing*, vol. 93, no. 1, 338-344.
- [18] J. M. Kim, O. K. Lee, and J. C. Ye, 2012. Improving noise robustness in subspace-based joint sparse recovery. *IEEE Transactions on Signal Process*, vol. 60, no. 11, 5799-5809.
- [19] M. Lai and Y. Liu, 2010. The null space property for sparse recovery from multiple measurement vectors. *Applied and Computational Harmonic Analysis*, vol. 30, 402-406.
- [20] K. Lee, Y. Bresler and M. Junge, 2012. Subspace methods for joint sparse recovery. *IEEE Transactions on Information Theory*, vol. 58, 3613-3641.

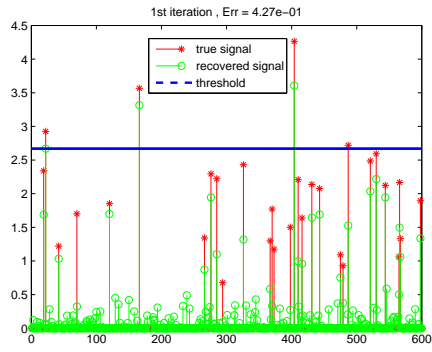
- [21] J. Liu, S. Ji, and J. Ye, 2009. SLEP: Sparse learning with efficient projections. Arizona State University, <http://www.public.asu.edu/~jye02/Software/SLEP>.
- [22] J. Liu, S. Ji, and J. Ye, 2009. Multi-task feature learning via efficient $\ell_{2,1}$ -norm minimization. In UAI 09 Proceedings of the Twenty-Fifth Conference on Uncertainty in Artificial Intelligence, 339-348.
- [23] H. Lu, X. Long, J. Lv, 2011. A fast algorithm for recovery of jointly sparse vectors based on the alternating direction methods. Proceedings of the 14th International Conference on Artificial Intelligence and Statistics (AISTATS), Fort Lauderdale, FL, USA, vol. 15.
- [24] J. Meng, W. Yin, H. Li, E. Hossian and Z. Han, 2011. Collaborative spectrum sensing from sparse observation in cognitive radio networks. IEEE Journal on Selected Areas in Communications, vol. 29, 327-337.
- [25] J. K. Nielsen, M. G. Christensen and S. H. Jensen, 2014. Joint sparsity and frequency estimation for spectral compressive sensing. IEEE International Conference on Acoustics, Speech and Signal Processing (ICASSP), 1035-1039.
- [26] G. Obozinski, B. Taskar and M. I. Jordan, 2007. Joint covariate selection for grouped classification. Technical report, Statistics Department, UC Berkeley.
- [27] J. Park, S. Hwang, D. Kim, and J. Yang, 2012. Utilization of partial common information in distributed compressive sensing. 2012 IEEE 75th Vehicular Technology Conference (VTC Spring), 1-5.
- [28] Z. Qin, K. Scheinberg, and D. Goldfarb, 2013. Efficient block-coordinate descent algorithms for the group lasso. Mathematical Programming Computation, vol. 5, 143-169.
- [29] T. S. Rappaport, 1996. Wireless Communications: Principles and Practice. Prentice Hall PTR New Jersey.
- [30] R. Tibshirani, 2013. The lasso problem and uniqueness. Electronic Journal of Statistics 7, 1456-1490.

- [31] A. Saleh, F. Alajaji, and W. Y. Chan, 2015. Compressed sensing with non-gaussian noise and partial support information. *Signal Processing Letters, IEEE*, vol. 22, no. 10, 1703-1707.
- [32] J. A. Tropp, A. C. Gilbert, and M. J. Strauss, 2006. Algorithms for simultaneous sparse approximation. Part I: Greedy pursuit. *Signal Process*, vol. 86, no. 3, 572-588.
- [33] Y. Wang and W. Yin, 2010. Sparse signal reconstruction via iteration support detection. *SIAM Journal on Imaging Sciences*, vol. 3, no. 3, 462-491.
- [34] Wimalajeewa, Thakshila and Varshney, Pramod K, 2014. OMP based joint sparsity pattern recovery under communication constraints. *IEEE Transactions on Signal Processing*, vol. 62, no. 19, 5059-5072.
- [35] S. Wright, R. Nowak, and M. Figueiredo, 2009. Sparse reconstruction by separable approximation. *IEEE Transactions on Signal Processing*, vol. 57, no. 7, 2479-2493.
- [36] J. Yang and Y. Zhang, 2009. Alternating direction algorithms for ℓ_1 -problems in compressive sensing. *SIAM Journal on Scientific Computing*, vol. 33, 250-278.
- [37] X. Yang, K. Seyoun, and P. X. Eric, 2009. Heterogeneous multitask learning with joint sparsity constraints. *Advances in Neural Information Processing Systems*.
- [38] X. Zhang, and C. Liu, 2013. A one-dimensional slope detection approach. *SpringerPlus*, vol. 2, no. 1, 474.
- [39] Z. Zheng and Y. Fan and J. Lv, 2014. High dimensional thresholded regression and shrinkage effect. *Journal of the Royal Statistical Society: Series B (Statistical Methodology)*, vol. 76, 627-649.
- [40] J. Zhou, J. Chen and J. Ye, 2012. MALSAR: Multi-task learning via structural regularization. Arizona State University. <http://www.public.asu.edu/~jye02/Software/MALSAR>.

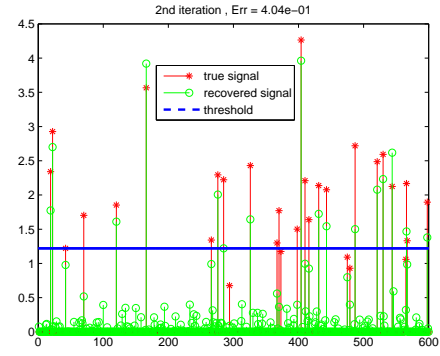


L-Iteration Number	Nonzeros				Relative error
	Total true	Detected	Correct	False	
1-1	30	37	29	8	6.26e-01
1-4	30	30	30	0	5.65e-05
2-1	30	34	28	6	3.73e-01
2-4	30	30	30	0	7.57e-05
4-1	30	38	30	8	2.78e-01
4-4	30	30	30	0	7.05e-05
8-1	30	34	30	4	2.82e-01
8-4	30	30	30	0	4.77e-05
16-1	30	33	30	3	2.80e-01
16-4	30	30	30	0	9.08e-05

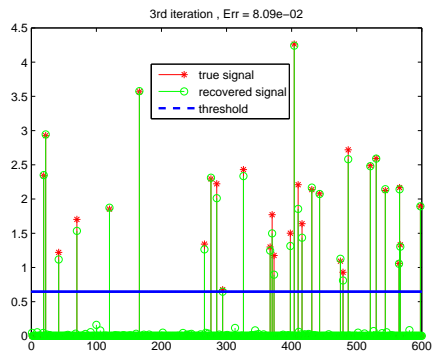
Figure 1: compare the true Gaussian signals and recovered signals from ISDJS in different channels, where the two parts in each subplot are the results in the first iteration and the fourth iteration from ISDJS, respectively. (a)L=1, m=120, (b)L=2, m=100, (c)L=4, m=80, (d)L=8, m=60, (e)L=16, m=60.



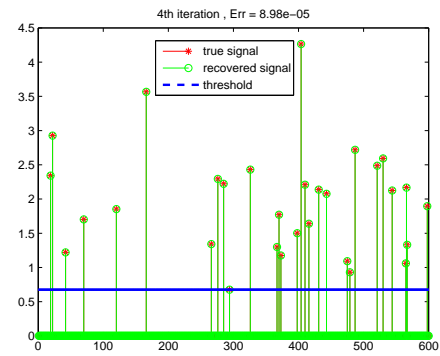
(a)



(b)



(c)



(d)

Iteration Number	Nonzeros				Relative error
	Total true	Detected	Correct	False	
1	30	41	27	14	4.27e-01
2	30	40	28	12	4.04e-01
3	30	30	30	0	8.09e-02
4	30	30	30	0	8.98e-05

Figure 2: compare the true Gaussian signals and recovered signals from ISDJS in each iteration in 4 channels case.

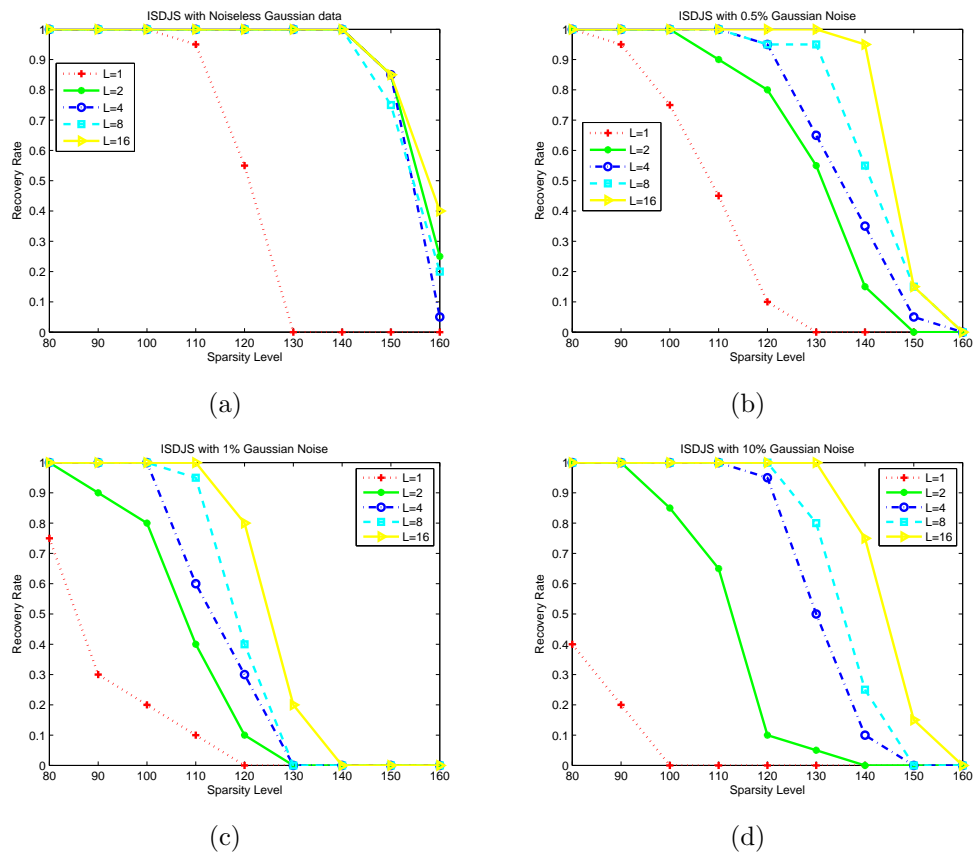
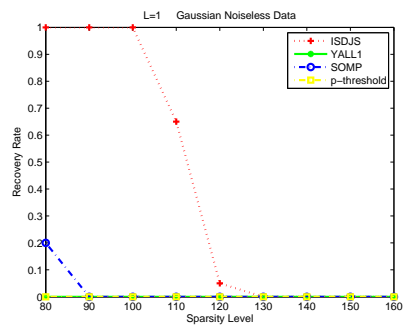
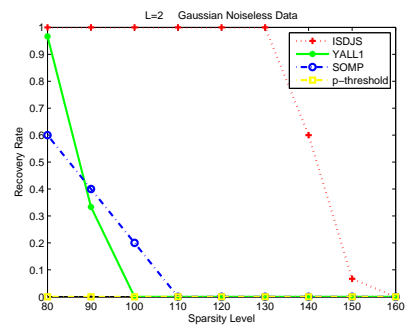


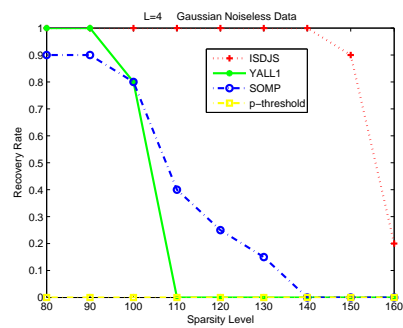
Figure 3: compare the recovery rate of ISDJS with $L=1, 2, 4, 8, 16$ in different noise levels for Gaussian signals, (a)noiseless data, (b)0.5% noise, (c)1% noise, (d)10% noise.



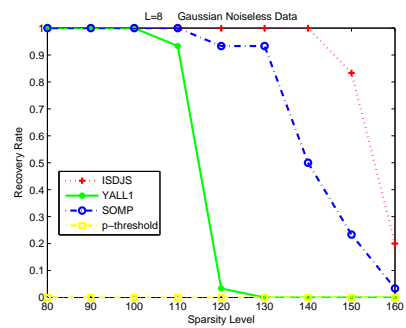
(a)



(b)

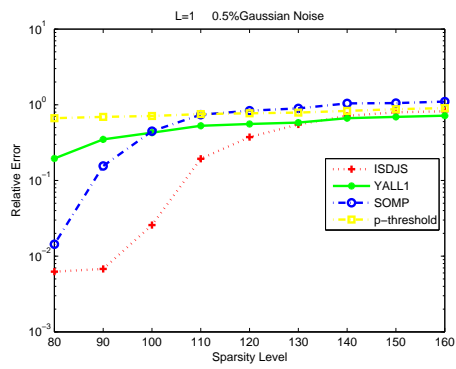


(c)

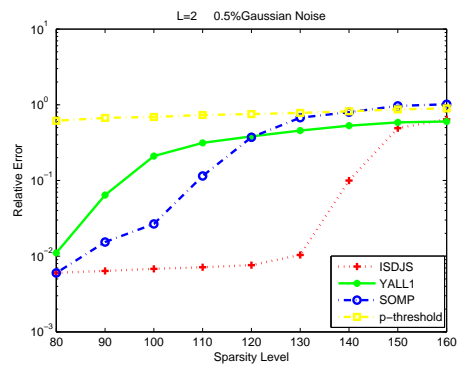


(d)

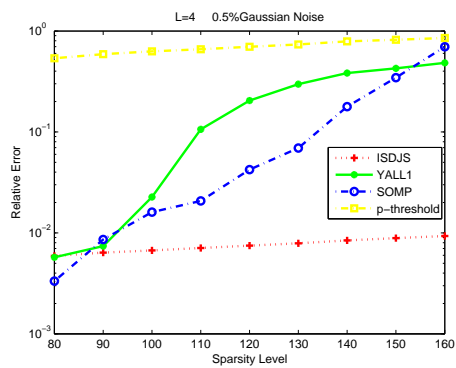
Figure 4: compare the recovery rate of four algorithms in different channels for noiseless Gaussian signals, (a) $L=1$, (b) $L=2$, (c) $L=4$, (d) $L=8$.



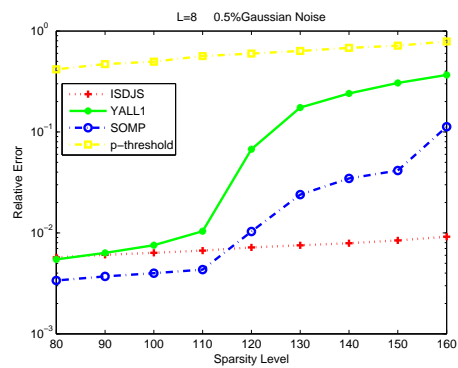
(a)



(b)

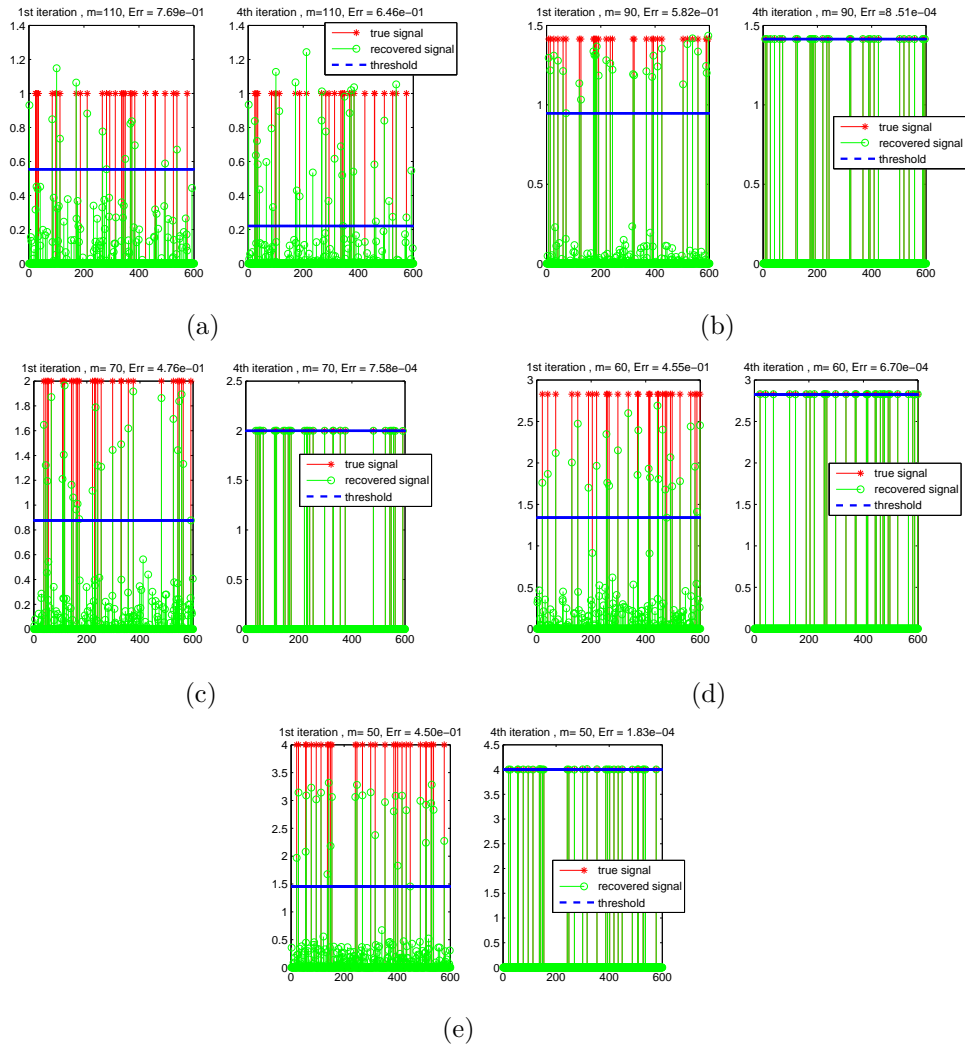


(c)



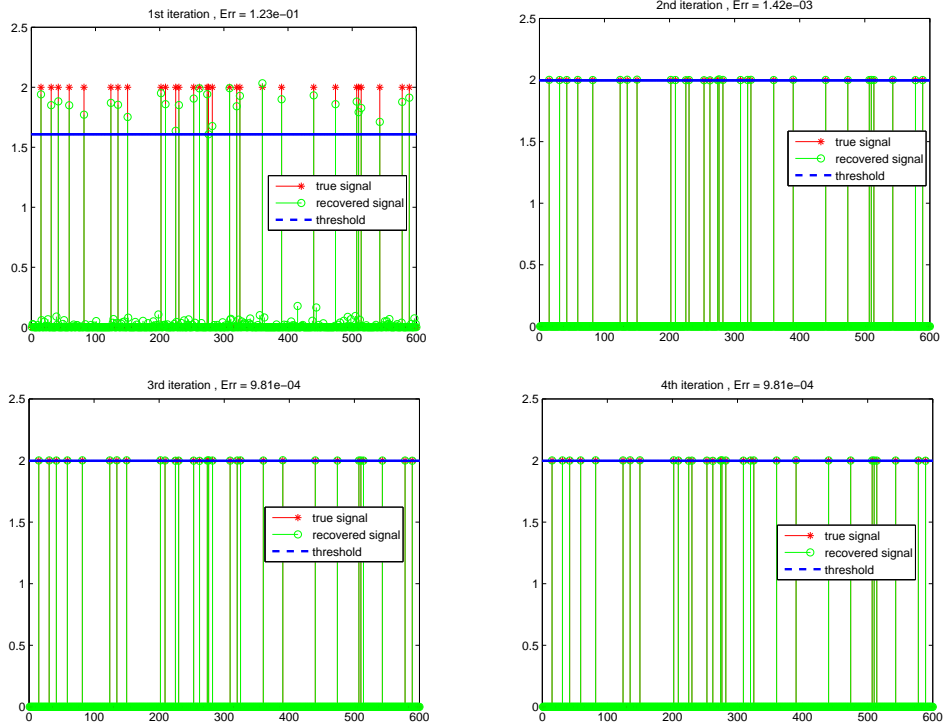
(d)

Figure 5: compare relative error of four algorithms in different channels with 0.5% noise for Gaussian signals, (a) $L=1$, (b) $L=2$, (c) $L=4$, (d) $L=8$.



L-Iteration Number	Nonzeros				Relative error
	Total true	Detected	Correct	False	
1-1	30	33	27	6	7.69e-01
1-4	30	36	30	6	6.46e-01
2-1	30	32	30	2	5.82e-01
2-4	30	30	30	0	8.51e-04
4-1	30	35	30	5	4.76e-01
4-4	30	30	30	0	7.58e-04
8-1	30	35	30	5	4.56e-01
8-4	30	30	30	0	6.70e-04
16-1	30	32	30	2	4.50e-01
16-4	30	30	30	0	1.83e-04

Figure 6: compare the true Bernoulli signals and recovered signals from ISDJS in different channels, where the two components in each subplot is the result in the first iteration and the fourth iteration from ISDJS, respectively. (a)L=1, m=110, (b)L=2, m=90, (c)L=4, m=70, (d)L=8, m=60, (e)L=16, m=50.



Iteration Number	Nonzeros				Relative error
	Total true	Detected	Correct	False	
1	30	28	26	2	1.23e-01
2	30	29	29	0	1.42e-03
3	30	30	30	0	9.81e-04
4	30	30	30	0	9.81e-04

Figure 7: compare the true Bernoulli signals and recovered signals from ISDJS in each iteration in the 4-channel cases.

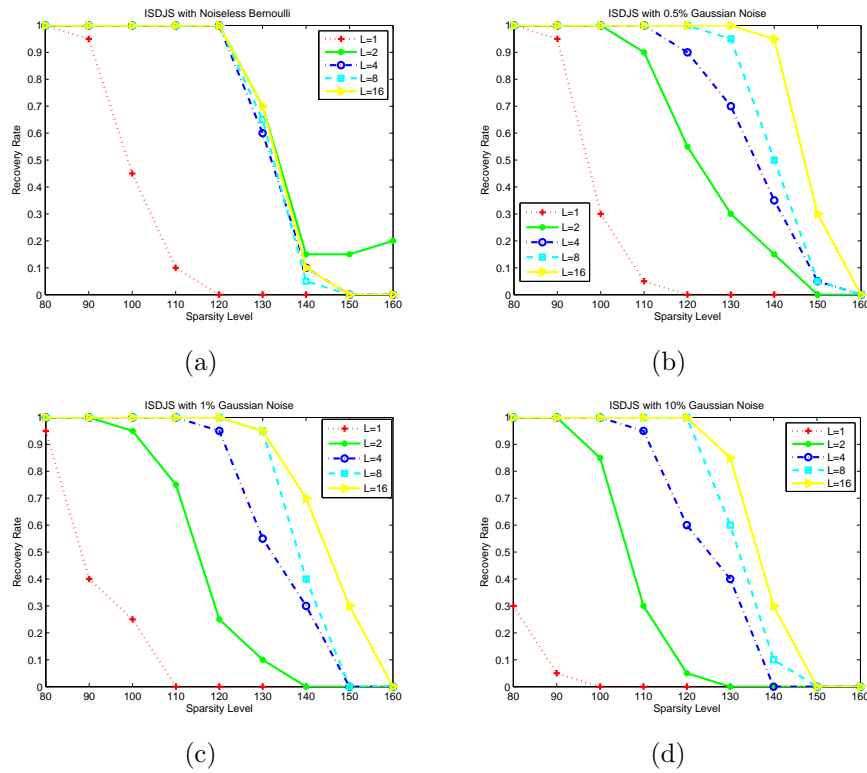
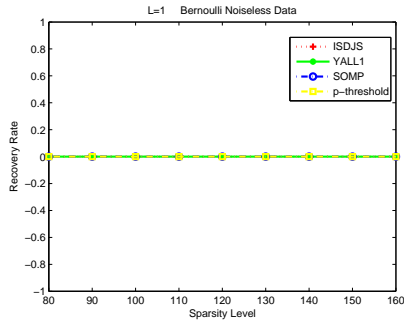
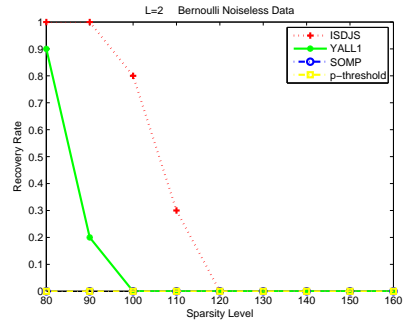


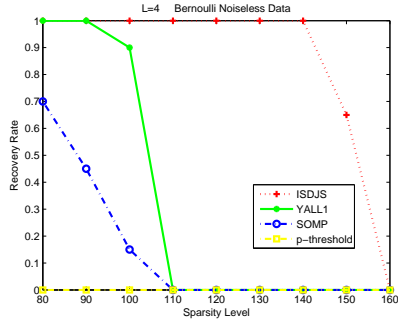
Figure 8: compare the recovery rate of ISDJS with $L=1, 2, 4, 8, 16$ in different noise levels for Bernoulli signals, (a) noiseless data, (b) 0.5% noise, (c) 1% noise, (d) 10% noise.



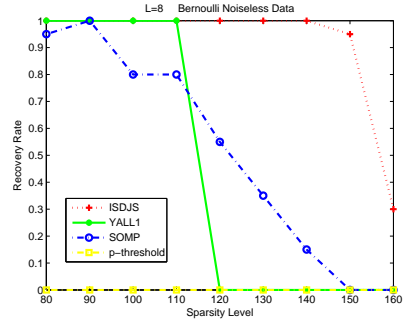
(a)



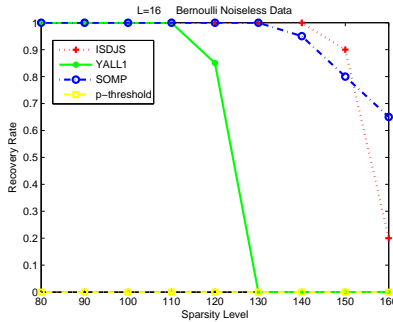
(b)



(c)

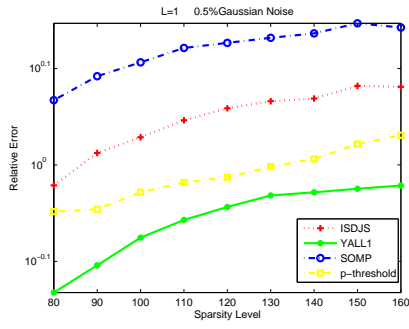


(d)

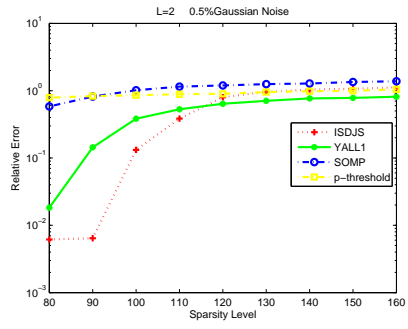


(e)

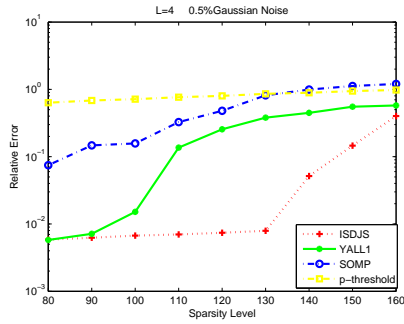
Figure 9: compare the recovery rate of four algorithms in different channels for noiseless Bernoulli signals, (a) $L=1$, (b) $L=2$, (c) $L=4$, (d) $L=8$, (e) $L=16$.



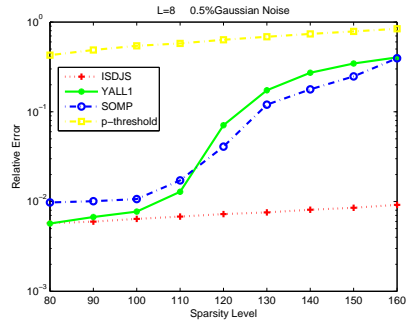
(a)



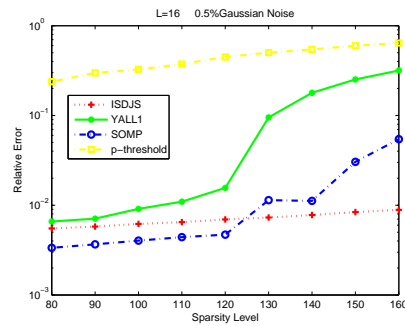
(b)



(c)



(d)



(e)

Figure 10: compare relative error of four algorithms in different channels with 0.5% noise for Bernoulli signals, (a) $L=1$, (b) $L=2$, (c) $L=4$, (d) $L=8$, (e) $L=16$.

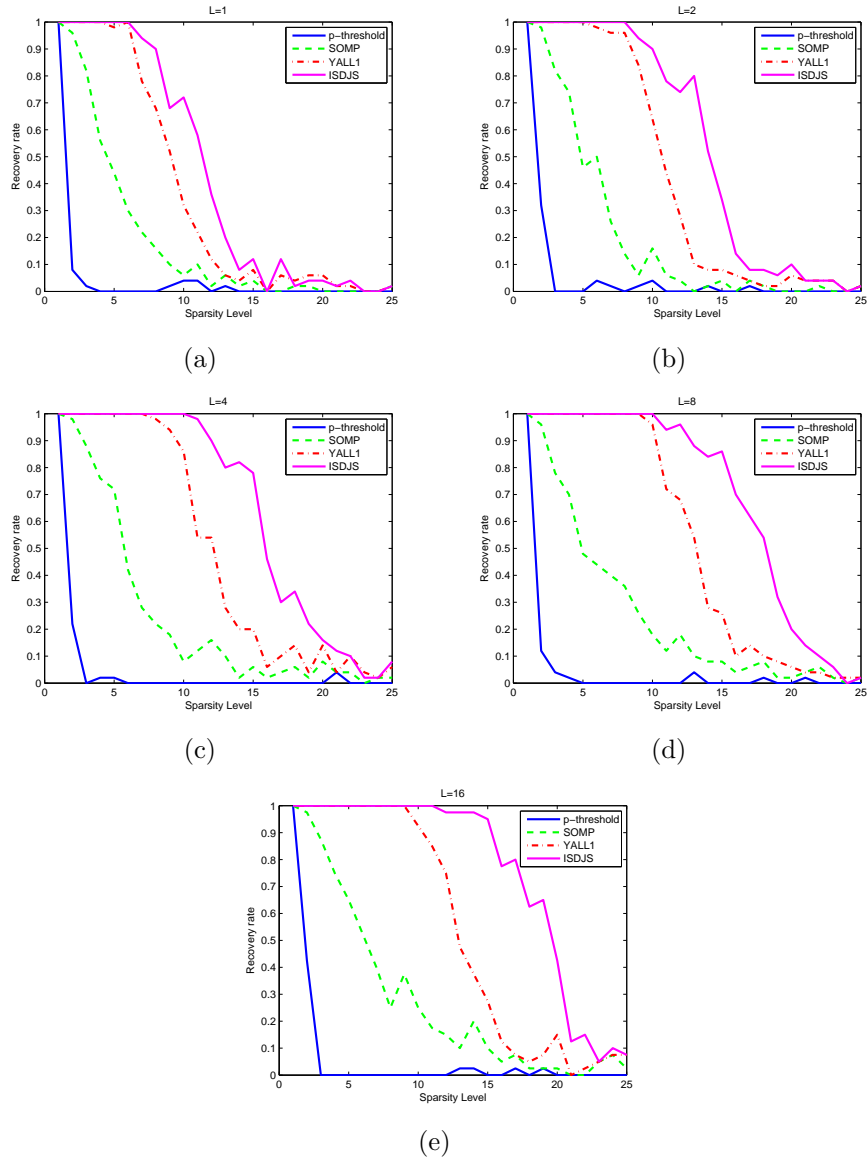


Figure 11: compare the recovery rate of four algorithms in different channel numbers in the example of spectrum sensing, (a) $L=1$, (b) $L=2$, (c) $L=4$, (d) $L=8$, (e) $L=16$.

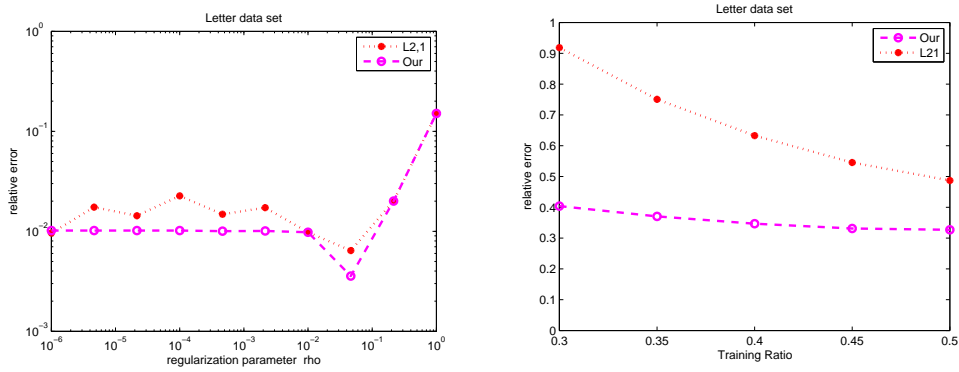


Figure 12: compare the algorithm of [22] with our proposed algorithm.